AGU PUBLICATIONS

JGR

Journal of Geophysical Research: Solid Earth

RESEARCH ARTICLE
10.1002/2016JB013632

**Key Points:**
- We relocated the original catalog event with TomoDD and identified linear dipping structure around the epicenter
- Using the matched filter technique, we identified about 17 times more aftershocks within the first 4 months
- We observed 53 repeating aftershock clusters, each with at least four events, and they majorly occurred along the interface

**Supporting Information:**
- Supporting Information S1
- Table S1
- Table S2
- Table S3
- Table S4

**Correspondence to:**
D. Yao,
dyao30@gatech.edu

**Citation:**
Yao, D., J. I. Walter, X. Meng, T. E. Hobbs, Z. Peng, A. V. Newman, S. Y. Schwartz, and M. Protti (2017), Detailed spatiotemporal evolution of microseismicity and repeating earthquakes following the 2012 $M_w$ 7.6 Nicoya earthquake, *J. Geophys. Res. Solid Earth*, *122*, 524–542, doi:10.1002/2016JB013632.

Received 8 OCT 2016
Accepted 31 DEC 2016
Accepted article online 4 JAN 2017
Published online 26 JAN 2017



# Detailed spatiotemporal evolution of microseismicity and repeating earthquakes following the 2012 $M_w$ 7.6 Nicoya earthquake

**Dongdong Yao[1], Jacob I. Walter[2,3], Xiaofeng Meng[4,5], Tiegan E. Hobbs[1], Zhigang Peng[1], Andrew V. Newman[1], Susan Y. Schwartz[6], and Marino Protti[7]**

[1]Earth and Atmospheric Sciences, Georgia Institute of Technology, Atlanta, Georgia, USA, [2]Oklahoma Geological Survey, University of Oklahoma, Norman, Oklahoma, USA, [3]Institute for Geophysics, University of Texas at Austin, Austin, Texas, USA, [4]Department of Earth and Space Sciences, University of Washington, Seattle, Washington, USA, [5]Science Institute, University of Washington, Seattle, Washington, USA, [6]Department of Earth and Planetary Sciences, Santa Cruz, California, USA, [7]Observatorio Vulcanológico y Sismológico de Costa Rica, Universidad Nacional, Heredia, Costa Rica

**Abstract** We apply a waveform matching technique to obtain a detailed earthquake catalog around the rupture zone of the 5 September 2012 moment magnitude 7.6 Nicoya earthquake, with emphasis on its aftershock sequence. Starting from a preliminary catalog, we relocate ~7900 events using TomoDD to better quantify their spatiotemporal behavior. Relocated aftershocks are mostly clustered in two groups. The first is immediately above the major coseismic slip patch, partially overlapping with shallow afterslip. The second one is 50 km SE to the main shock nucleation point and near the terminus of coseismic rupture, in a zone that exhibited little resolvable afterslip. Using the relocated events as templates, we scan through the continuous recording from 29 June 2012 to 30 December 2012, detecting approximately 17 times more than template events. We find 190 aftershocks in the first half hour following the main shock, mostly along the plate interface. Later events become more scattered in location, showing moderate expansion in both along-trench and downdip directions. From the detected catalog we identify 53 repeating aftershock clusters with mean cross-correlation values larger than 0.9, and indistinguishably intracluster event locations, suggesting slip on the same fault patch. Most repeating clusters occurred within the first major aftershock group. Very few repeating clusters were found in the aftershock grouping along the southern edge of the Peninsula, which is not associated with substantial afterslip. Our observations suggest that loading from nearby afterslip along the plate interface drives spatiotemporal evolution of aftershocks just above the main shock rupture patch, while aftershocks in the SE group are to the SE of the observed updip afterslip and poorly constrained.

## 1. Introduction

Subduction zones are responsible for the largest earthquakes along the megathrust fault defining the plate boundary, sometimes with moment magnitudes ($M_w$) exceeding 8.0 and causing considerable destruction. With better station coverage and advanced processing techniques, many recent studies have shown that megathrust earthquake ruptures normally initiate within the frictionally unstable region at seismogenic depth but can propagate both downdip and updip into conditionally stable regions [e.g., *Lay*, 2015]. In these conditionally stable regions, slow-slip events (SSEs) have been observed by geodetic and/or seismic instruments at many subduction megathrusts, including the northern Costa Rica Pacific margin [e.g., *Schwartz and Rokosky*, 2007; *Dixon et al*., 2014]. While small asperities in conditionally stable regions are capable of generating a range of seismic behaviors, including microearthquakes, low-frequency earthquakes (LFEs), and deep tectonic tremors [*Beroza and Ide*, 2011; *Peng and Gomberg*, 2010], the physical conditions controlling locked asperities and the degree to which the surrounding fault accommodates and releases strain remain largely unknown. These processes have implications for better understanding the accommodation and release of tectonic stresses on a larger scale that sometimes coalesce and grow into great earthquakes.

Large earthquakes are known to trigger additional earthquakes both in the near and far field [e.g., *King and Devès*, 2015; *Hill and Prejean*, 2015]. There are a variety of ways that earthquakes trigger other earthquakes. Positive (or negative) Coulomb stress changes estimated for nearby or adjacent receiver faults, induced by main shock static slip, are sometimes consistent with either increases or decreases in seismicity, depending on event or locale [e.g., *King et al*., 1994; *Stein et al*., 1994, 1997]. This is complicated by the fact that some of

these effects may be delayed in time. In cases of purported delayed triggering, a closer examination of time-dependent stress transfer mechanisms is needed to understand the delayed triggering mechanism [*Freed*, 2005]. One mechanism proposed for direct earthquake triggering suggests earthquakes trigger as cascading failures with prior earthquakes promoting new earthquakes on nearby faults [*Felzer et al*., 2003]. Other mechanisms generally involve postseismic stress changes. These include viscous relaxation primarily in the asthenosphere [*Kirby and Kronenberg*, 1987], poroelastic rebound when excess fluid pressures recover to their prequake state [*Peltzer et al*., 1998; *Masterlark and Wang*, 2002], and afterslip where the unrelieved accumulated strain on the fault causes aseismic slip along the fault surrounding the coseismic slip patch [*Marone*, 1998; *Hearn et al*., 2002].

Previous studies on aftershock triggering mostly utilize earthquakes listed in standard seismic data center or observatory monitoring catalogs [e.g., *Toda et al*., 2012]. However, those aftershock catalogs suffer from missing events due to their high rate of occurrence, causing both overlapping signals and analyst or methodological overload from the overall large number of events. The majority of masked, smaller events are early aftershocks within the surface/coda waves from the main shock, or following particularly large aftershocks [e.g., *Kagan*, 2004; *Peng et al*., 2006, 2007]. A common solution to identify those missing earthquakes is the network waveform matched filter technique (NWMFT) [*Gibbons and Ringdal*, 2006], which utilizes the fact that earthquakes produce similar waveforms if both focal mechanism and paths are similar, and source durations are sufficiently short. Thus, instead of relying on more traditional detection functions, including short-term-average/long-term-average (STA/LTA) amplitudes [*Allen*, 1982], the NWMFT employs the waveform similarity to identify new events by cross-correlating clear *P* and *S* waveforms from existing catalog events with continuous recordings. The method is suitable over a range of magnitudes and can identify both very small events with very low signal-to-noise ratios (SNR). The method was used to identify LFEs within continuous tremor [*Shelly et al*., 2007] and was later widely adopted to detect missing aftershocks, foreshocks, induced earthquakes, and remotely triggered seismicity around recent large earthquakes [*Peng and Zhao*, 2009; *Meng et al*., 2013; *Kato et al*., 2012; *Kato and Nakagawa*, 2014; *Wu et al*., 2014; *Skoumal et al*., 2014; *Walter et al*., 2015; *Yao et al*., 2015].

In this study, we analyzed available seismic data around the 5 September 2012 $M_w$ 7.6 Nicoya earthquake in Costa Rica. The existence of the Nicoya Peninsula enables very near-field seismic and geodetic observations of megathrust seismogenesis, as it brings the coastline within 50 km of the trench, allowing land-based geophysical studies directly over the main locking and slip environment, while the seismogenic zones exist entirely offshore in most environments. As anticipated, the Nicoya earthquake ruptured a seismic gap beneath the Nicoya Peninsula that locked up following a *M* 7.7 event in 1950 and exhibiting an apparent 50–60 year recurrence of $M_w$ 7.0+ earthquakes along the megathrust [*Protti et al*., 2001]. After nucleating immediately offshore [*Yue et al*., 2013], the Nicoya earthquake ruptured primarily under the peninsula with up to 4 m of trenchward thrust in an area that was previously mapped as locked [*Feng et al*., 2012; *Protti et al*., 2014; *Kyriakopoulos and Newman*, 2016]. Local foreshocks were observed 35 min prior to the main shock within 15 km of its hypocenter, which occurred within the same 30 km diameter zone as those remotely triggered by the 27 August 2012 $M_w$ 7.3 El Salvador event about 450 km to the northwest [*Walter et al*., 2015]. *Kyriakopoulos et al*. [2015] derived a new structural model for the subduction zone interface along the Middle America Trench. This plate geometry model was further used to reevaluate the interseismic locking and coseismic slip [*Kyriakopoulos and Newman*, 2016] and image afterslip both updip of the dominant coseismic slip area and downdip to deep slow-slip events previously identified [*Hobbs et al*., 2016].

As an extension of the growing body of work in the area, we explored the detailed spatiotemporal evolution of aftershocks along the Nicoya megathrust using the NWMFT to better understand physical mechanisms of aftershock triggering and how megathrust faults recover in the postseismic period. In addition, we searched for potential repeating earthquakes with virtually identical waveforms [e.g., *Nadeau et al*., 1995; *Peng and Ben-Zion*, 2006] and used them to better understand postseismic deformation [*Schaff et al*., 1998; *Peng et al*., 2005; *Kato and Igarashi*, 2012].

## 2. Study Region and Seismic Data

With land directly on top of the seismically active subduction interface, the Nicoya Peninsula is an ideal place to study megathrust slip processes. Besides regular earthquakes, both shallow and deep SSEs [*Jiang et al*., 2012; *Dixon et al*., 2014], as well as tectonic tremors/LFEs, have been identified in this region [*Brown et al*.,

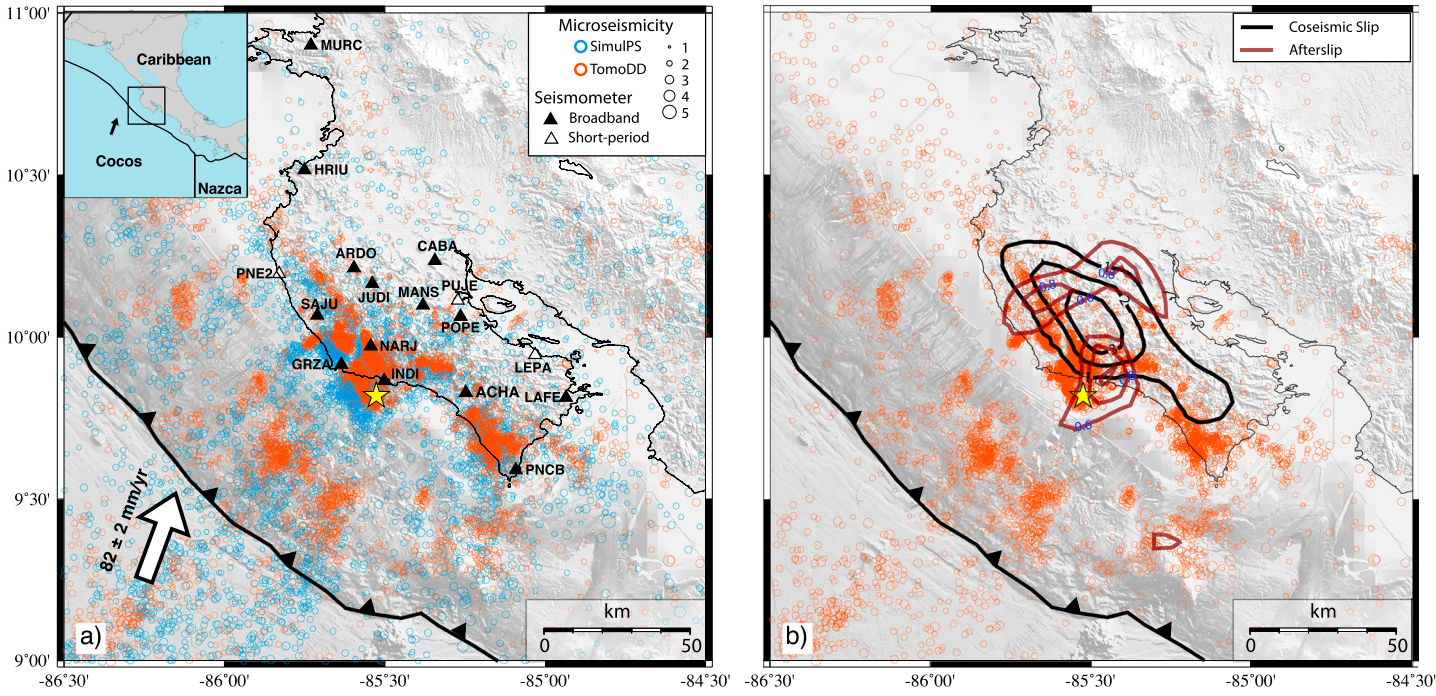


**Figure 1.** Map of the Nicoya Peninsula, Costa Rica (study region). (a) Seismic network (triangles) and earthquake catalog using SimulPS (blue circles) [*Walter et al.*, 2015], and TomoDD (red circles), following the methodology and model described in *Kyriakopoulos et al.* [2015]. Inset shows the regional tectonic environment including Cocos plate subduction beneath the Caribbean plate at about 82 ± 2 mm/yr near Nicoya [*Demets et al.*, 2010]. (b) The TomoDD seismicity is shown with the geodetically inferred coseismic slip (1 m thick black contours) [*Kyriakopoulos and Newman*, 2016] and postseismic deformation modeled as afterslip through the end of 2012 (0.25 m maroon contours starting at 0.5 m) [*Hobbs et al.*, 2016]. The yellow star marks the main shock epicenter. The geodetic slip models both use the seismically defined 3-D slab structure of *Kyriakopoulos et al.* [2015].

2009; *Walter et al.*, 2011, 2013], demonstrating a broad spectrum of fault slip phenomena [*Peng and Gomberg*, 2010]. The smoother and colder Cocos plate originating from the East Pacific Rise subducts beneath the Peninsula to the north, while the rougher (with many seamounts) and warmer seafloor created at Cocos-Nazca Spreading center converges with the Caribbean plate to the south with an average rate of 82 mm/yr in the N20°E direction (Figure 1a) [*DeMets et al.*, 2010]. This is consistent with the along-strike variation in the updip limit of the seismogenic zone and strong variations in the megathrust interface structure [*Newman et al.*, 2002; *Kyriakopoulos et al.*, 2015], as well as an along-strike variation in the temperature profile of the incoming oceanic plate [*Harris and Wang* 2002; *Hutnak et al.*, 2007].

During the past two decades, numerous seismic and geodetic instruments were deployed in this region [*Dixon et al.*, 2013]. Geodetic instruments are composed of campaign and continuous GPS sites initiated in the early 1990s [*Lundgren et al.*, 1999]. These data were instrumental in imaging interseismic coupling with strong along-strike variability along the subducting interface [*Feng et al.*, 2012], which were used to estimate the potential location and maximum moment release for the impending 2012 Nicoya earthquake [*Protti et al.*, 2014].

Starting with a 1.5 year deployment by the University of California, Santa Cruz (UCSC) of 20 short-period and broadband sensors beginning in late 1999, the Nicoya Peninsula has been well instrumented with seismometers to date. The current network YZ has remained relatively unchanged since 2008 (Figure 1a) and consists of a 17-station seismic network operated by UCSC, Georgia Tech, and the Costa Rica Volcanological Observatory at the National University providing continuous recordings before, during, and after the 2012 Nicoya main shock [*Dixon et al.*, 2013]. The network consists of 14 broadband and three short-period sensors recording initially at between 40 and 50 and currently at 100 samples per second. As shown in Figure S1 in the supporting information, about 10 stations were working continuously immediately following the main shock.

In this study, we analyzed data between July and December 2012, about 2 months before and 4 months following the $M_w$ 7.6 main shock. The cataloged events were first identified within the Antelope seismic database system (http://www.brtt.com) using an automatic detection algorithm followed by analyst revision of

phase picks [*Walter et al*., 2015]. Events were then relocated with SimulPS [*Evans et al*., 1994] by incorporating available phase arrivals with a regionally developed tomographic 3-D velocity model [*DeShon et al*., 2006] (Figure 1a). Finally, we selected 7890 earthquakes with at least six known phase arrivals for further analysis, hereafter we refer to these as the "original catalog." *Walter et al*. [2015] used a NWMFT on this initial catalog to identify dynamic triggering by the 2012 El Salvador earthquake near the nucleation region of the Nicoya earthquake and look for foreshock activities. This study is distinguished from the earlier one in that it focuses on the aftershock (postmain shock) seismicity.

## 3. Methods

### 3.1. Phase Detection and Catalog Relocation

Beginning with raw waveforms from the original catalog, we filtered them between 2 and 15 Hz to suppress noise from regional and teleseismic events as well as background noise with dominantly low-frequency energy. Additional phases were then identified using an automatic phase picker that repeatedly predicts arrivals with an initial velocity model, searches for phases using detector functions, and inverts the new velocity model [*Li and Peng*, 2016], with additional manual phase picking and adjustment (Figure S2). We then applied the new phase information to relocate events within *TomoDD* [*Zhang and Thurber*, 2003]. Both the absolute and differential times were used to better constrain their relative locations.

In detail, we first used the *ph2dt* program [*Waldhauser and Ellsworth*, 2000] to obtain differential travel times by searching catalog *P* and *S* phases for event pairs at common stations. We optimized the connectivity between events by selecting well-linked pairs and removing outliers when their delay times were larger than the maximum expected value of 5 s. The parameters were optimized for the network geometry and seismicity distribution, where 10 km was chosen as the maximum hypocentral separation between event pairs and a minimum of eight links required for clustering. The new travel times were utilized in TomoDD, including the most updated 3-D velocity model in this region [*Moore-Driskell et al*., 2013], to obtain the best constrained locations.

### 3.2. Matched Filter Detection

The relocated events were then used as templates to perform the matched filter detection. The procedure follows those in *Meng et al*. [2013] and is briefly described here. Since epicentral distances are generally within 150 km, we used a 6 s window (1 s before and 5 s after) around the *P* and *S* waves for vertical and horizontal channels separately and used them to compute cross-correlation (CC) functions with continuous data. To avoid noisy traces and suppress artificial detections, we computed the SNR for all traces by taking 1 s before and 5 s after the *P* or *S* arrival time as the signal window and the same length window ending 1 s before the *P* arrival as the noise window. Only template events having more than nine traces with SNRs greater than 5 were used. Next, we shifted each CC function for individual components back to the origin time of the templates and stacked all shifted functions to suppress uncorrelated background noise and enhance earthquake signals. We distinguished an event as a new earthquake detection if the stacked CC function exceeds a threshold of 12 times median absolute deviation (MAD) of daily mean CC functions, a threshold similar to previous studies [e.g., *Meng et al*., 2013; *Meng and Peng*, 2014; *Yao et al*., 2015; *Li et al*., 2016]. We then combined all detections and removed duplicates by keeping only the highest CC event per 3 s window [*Peng and Zhao*, 2009; *Meng et al*., 2013]. Finally, the locations of the detected events were assigned the same location as the best-matching template. The local magnitudes ($M_L$) of the detected events were computed by the median peak amplitude ratio between the template and detected events [*Peng and Zhao*, 2009]. Figure 2 illustrates a positive detection where an $M_L$ 2.4 event was detected at about 5 h following the main shock (at 19:47:35 on 5 September 2012) using an $M_L$ 3.1 template about 7 h later (at 02:21:35 on 6 September 2012).

### 3.3. Repeating Earthquakes

We then searched for repeating event pairs, defined as those with mean CC values higher than 0.9, excluding self-detections [e.g., *Kato et al*., 2012]. If an event is detected by multiple templates with CC $>$ 0.9, all the templates and corresponding CC values are kept. Next, we grouped the event pairs into clusters using an equivalency class (EC) algorithm [*Press et al*., 1986; *Peng and Ben-Zion*, 2005], which allows an inclusion of a new event into a cluster if the new event has a mean CC value $>$ 0.9 with any existing members in that cluster.

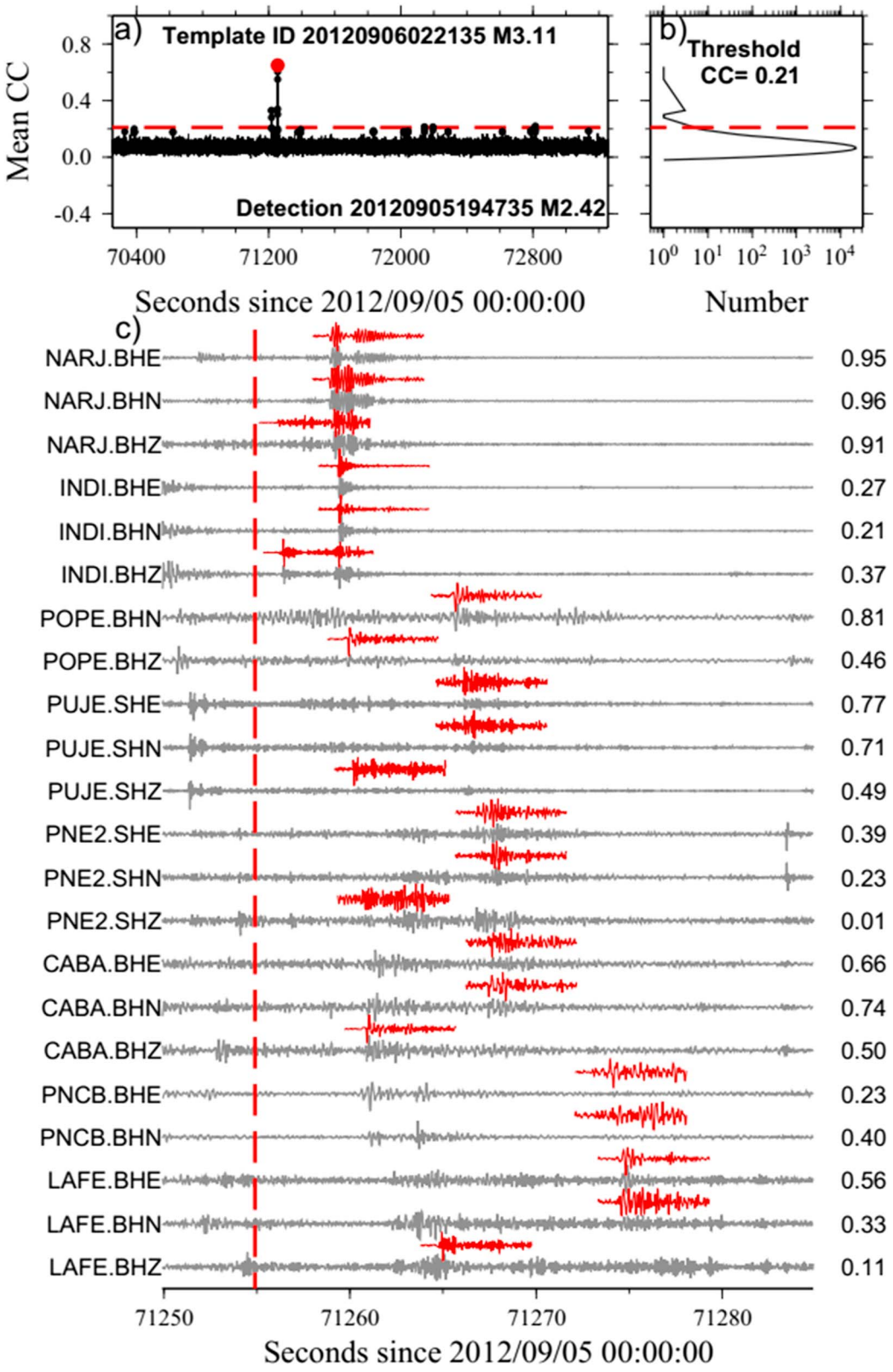


**Figure 2.** Illustration of a positive detection using the matched filter technique. A magnitude 2.4 event (origin time 5 September 2012 19:47:35) occurring 5 h after the main shock was detected by template 20120906022135 (M3.1). (a) Time series of cross correlations (CC) for a stacked trace encompassing the identified matched event (with CC = 0.65). (b) Histogram of CC value distribution for the window shown in Figure 2a. (c) Comparison of the waveforms peak match (gray) in Figure 2a with the template event (red). Station NAME.CHANNEL and corresponding individual CC values are marked on left and right sides, respectively.

As mentioned above, we relocated all 7890 catalog events using only catalog phases in TomoDD with a refined 3-D velocity model, which could help to constrain both the absolute and relative locations. We did not combine with waveform cross-correlation differential time mainly because the catalog includes events across a wide region, and it would cause more computation cost when compared to the potential improvements on relative relocations. On the other hand, to confirm whether events have overlapping rupture patches within each cluster, we further relocated them in *HypoDD* [*Waldhauser and Ellsworth*, 2000] with a simple 1-D velocity model by applying waveform cross-correlation differential time with subsample accuracy to reduce relative location errors [*Schaff et al*., 2002]. To estimate the patch size, we assumed an average strain drop of $10^{-4}$ [*Kasahara*, 1981], a circular crack model [*Kanamori and Anderson*, 1975; *Ben-Zion*, 2003], and an empirical potency-magnitude relationship for earthquakes with magnitudes $M < 3.5$ [*Ben-Zion and Zhu*, 2002].

$$r^3 = \left(7/16\right)\left(P_0/\Delta\varepsilon\right)$$
$$\log P_0 = 1.00M - 4.72 \tag{1}$$

where $r$ is the circular radius (in meters), $P_0$ is the scalar potency (in $\mathrm{km}^2 \times \mathrm{cm}$), and $\Delta\varepsilon$ is the static strain drop. Any events that were clearly outside the rupture patches of others were either dropped or separated into different subclusters. Finally, we estimated the amount of cumulative seismic slip for each cluster. Specifically, seismic slip for every event was calculated with aforementioned scalar potency and rupture area (assuming circular crack):

$$d = \frac{P_0}{(\pi r^2)} \tag{2}$$

where $d$ is the averaging seismic slip. Finally, we summed the clustered events to obtain the cumulative slip within each cluster.

## 4. Results

### 4.1. TomoDD Relocation Results

We were able to relocate approximately 7750 events from 19 June 2012 to 30 December 2012 (Figure 1; Table S1), while the rest 140 events were dropped by the TomoDD program. The relocated events formed two broad groups approximately 50–60 km in diameter beneath the western coast of the Nicoya Peninsula (Figure 1b). The first one is located along the terminus of the major coseismic slip patch, which partially overlaps shallow afterslip through the end of 2012 [*Hobbs et al*., 2016]. The second group of seismicity is near the southern edge of the peninsula, where little resolvable afterslip was observed.

To explore the depth distribution of relocated events, we plot the seismicity along several trench-normal (N45°E) cross sections (Figure 3). The seismicity to the northwest of and around the main shock epicenter (e.g., Figures 3b, 3d, 3e, and 3f) clearly outlines a linear feature that dips between 14 and 20° to the northeast. However, seismicity further south (e.g., Figures 3g, 3h, and 3i) appears more diffuse and does not seem to be on any linear interface.

We also observed along-strike variation of seismicity when plotting the depth distribution along the trench-parallel (N45°W) direction (Figure S3). The updip limit of the seismicity changed from ~20 km at depth in the northwest to shallower portion (~10 km depth) in the southeast, consistent with observations from the Costa Rica Seismogenic Zone Experiment (CRSEIZE) [*Newman et al*., 2002].

### 4.2. Earthquake Detection Results

We cross correlated the waveforms of 7750 relocated events with continuous recordings from 29 June 2012 to 30 December 2012. After the analysis, ~132,900 new events were detected (Figure 4 and Table S2). This includes ~129,800 events with robust magnitude determinations and ~3100 events with unreliable magnitudes. The unreliable event magnitudes are the results of templates without valid magnitudes from Antelope, which occurs when the SNR is lower than 3 for an individual phase. These are typically events with low magnitudes, and we arbitrarily assign them a magnitude of 0 in Figure 4 but did not use those events in subsequent analysis. The magnitude of completeness ($M_c$) drops from 2.0 for original catalog to 1.3 after including all detected events (Figure S4). A clear increase of seismicity was observed immediately following

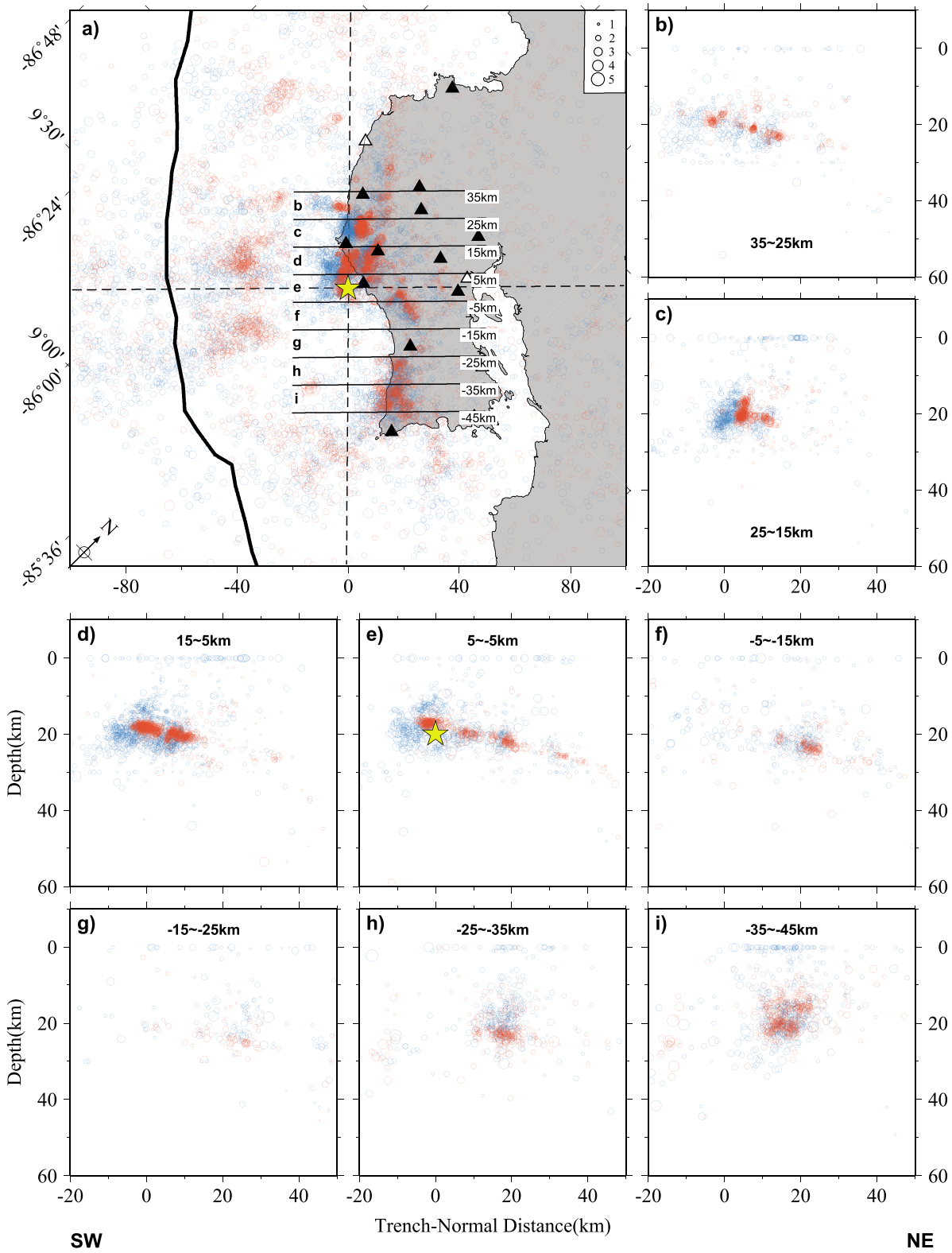


**Figure 3.** Details of relocated earthquake distribution. (a) All events projected along N45°E, the approximate trend of the Middle America Trench offshore Nicoya, with the *x* axis describing the position (in km) relative to the main shock epicenter (yellow star at −85.527°, 9.819°). Seismicity located using SimulPS (blue circles) [*Walter et al.*, 2015] are shown with TomoDD relocations (red circles) found using a local three-dimensional velocity model [*Moore-Driskell et al.*, 2013]. Trench-normal lines representing the bounds on profile bins (marked corresponding to their panel) are labeled with their trench-parallel distances from the main shock epicenter. (b–i) The depth profile within each bin. In Figure 3e the bin includes the focus of the main shock (depth = 20 km).

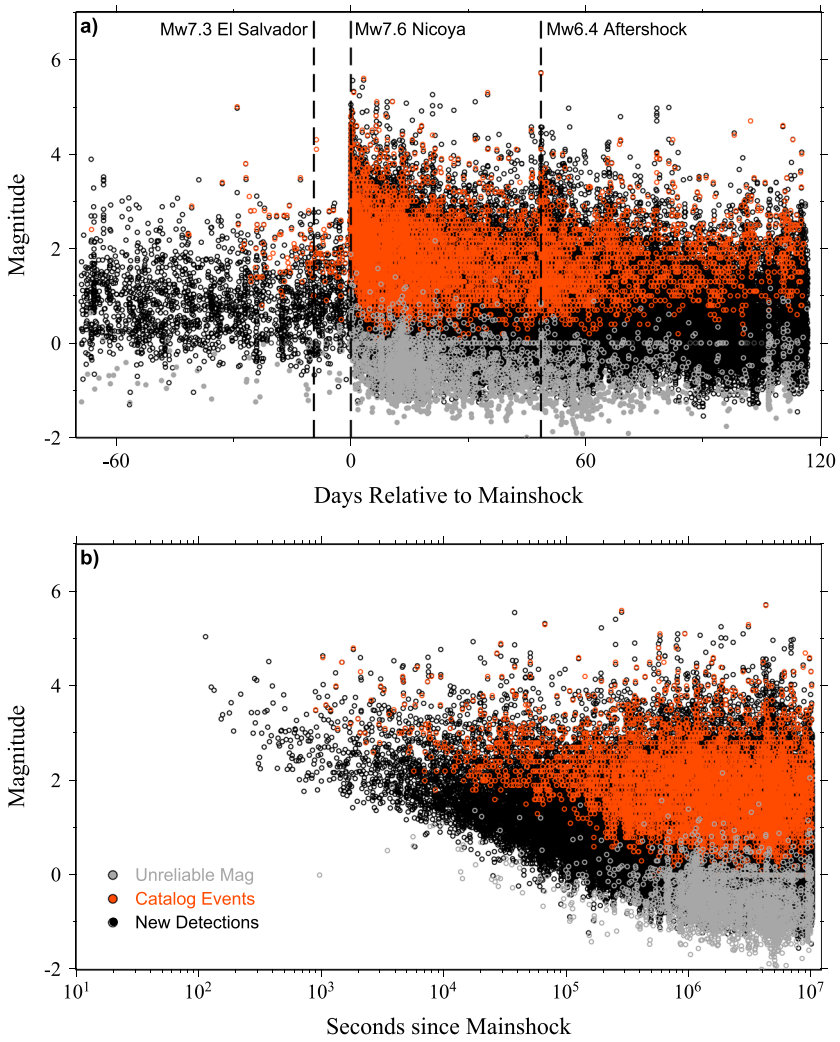


**Figure 4.** Time series of the waveform matching catalog. (a) Magnitude distribution with linear time scale for all detections from 29 June 2012 to 30 December 2012. (b) Aftershock magnitude distribution with logarithmic time since the main shock. Red and dark circles represent catalog template events and newly detected events, while gray circles mark catalog events without reliable magnitude and the associated detected events.

the main shock as well as after its largest aftershock (Figure 4a). In addition, we also observed an increase of local seismicity following the 2012 $M_w$ 7.3 El Salvador event, which was interpreted as remotely triggered seismicity in the epicentral region of the Costa Rica main shock [*Walter et al.*, 2015]. Figure 4b shows a clear reduction of the magnitude of the smallest event with logarithmic times since the main shock. It is worth noting that while the overall $M_c$ value is 1.3, this value is much higher immediately after the main shock. This is commonly observed right after moderate to large earthquakes [e.g., *Peng and Zhao*, 2009; *Tang et al.*, 2014] and is most likely caused by missing small earthquakes immediately following the main shock when the seismicity rate is high [*Hainzl*, 2016], even after matched filter detection.

We projected all events to both trench-parallel and trench-normal directions, in the same way as Figures 3 and S3, to further examine the spatiotemporal evolution of seismicity following the main shock in three adjacent time windows: 0–0.1 h, 0.1 h–0.5 h, and 0.5 h–5 h (Figure 5). We found that the earliest aftershocks (i.e., in the first half hour) occurred right around the main shock slip patch along the interface at the depth range of about 15–30 km (Figures 5a and 5b). Such a pattern is barely visible in the original catalog with only a few events in the first half hour after the main shock (Figure 5d). In comparison, the majority of aftershocks occurring further to the southeast near the tip of the Peninsula activates slightly later.

To better define the aftershock expansion pattern, we followed recent work by *Kato and Obara* [2014] and defined the activation of aftershocks at the time when the cumulative numbers of aftershocks within a

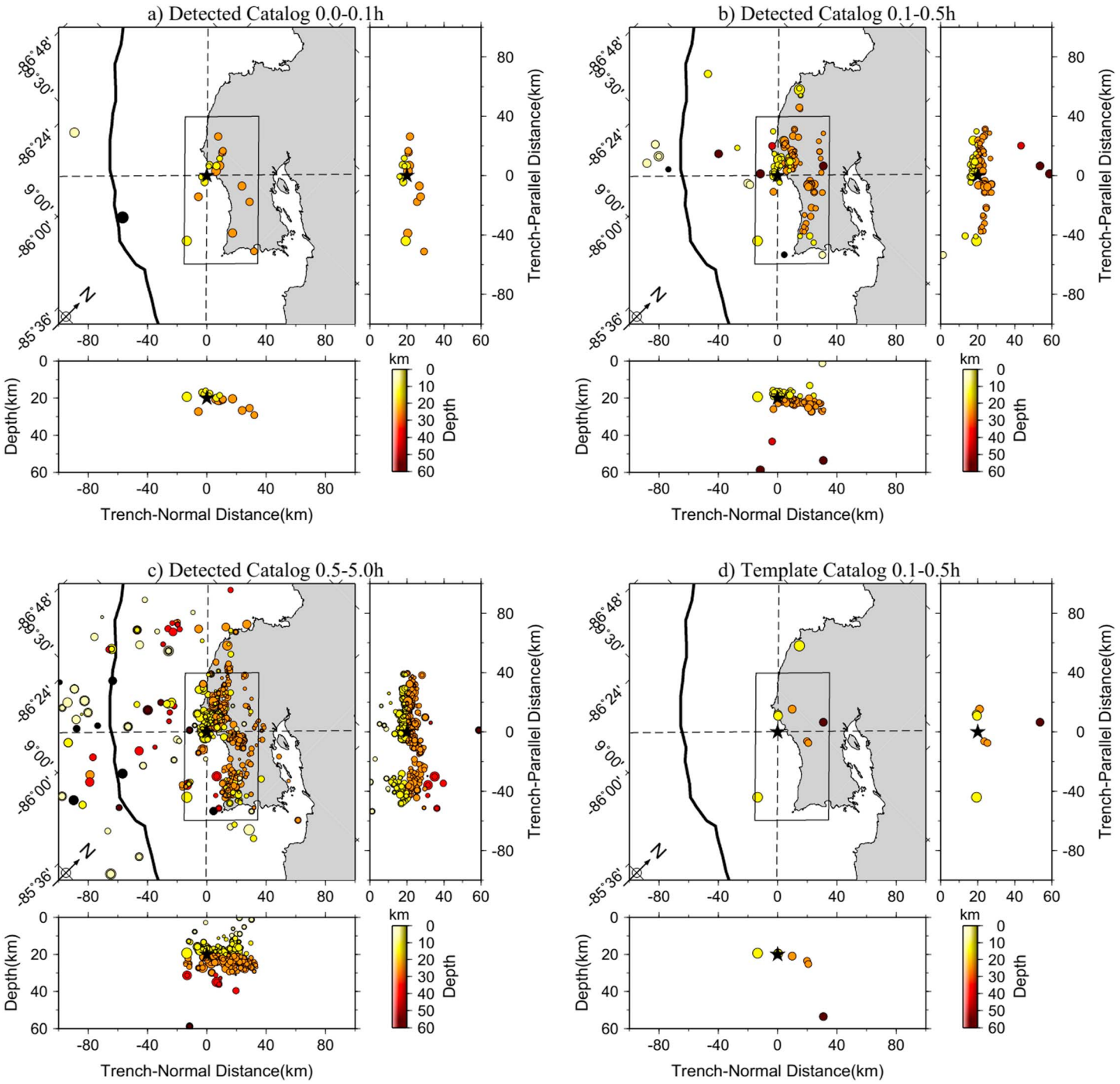


**Figure 5.** Spatiotemporal evolution of early aftershocks. Each panel shows a different time window following the main shock, where the top left is a map view of seismicity after a 45° clockwise rotation, and the trench-normal and trench-parallel distributions within the shown box are plotted at the bottom and to the right, respectively. Events are color coded with depth. Following the main shock the individual panels show (a) 0–0.1 h for the detected catalog; (b) 0.1–0.5 h for the detected catalog; (c) 0.5–5 h for the detected catalog; and (d) 0.1–0.5 h for the template catalog.

5 km wide zone (either along or perpendicular to the trench) exceed a certain number *N*. We slid the window per 1 km in order to achieve a better spatial resolution. As shown in Figure 6 ($N = 30$), both groups showed moderate expansion in trench-parallel and normal distances with logarithmic times since the main shock. We also set $N = 10$, 20, 30, 40, 50 to examine how the choice of such parameter affected the results, and they showed similar patterns. In addition, there was a gap between the seismicity beneath the Peninsula and

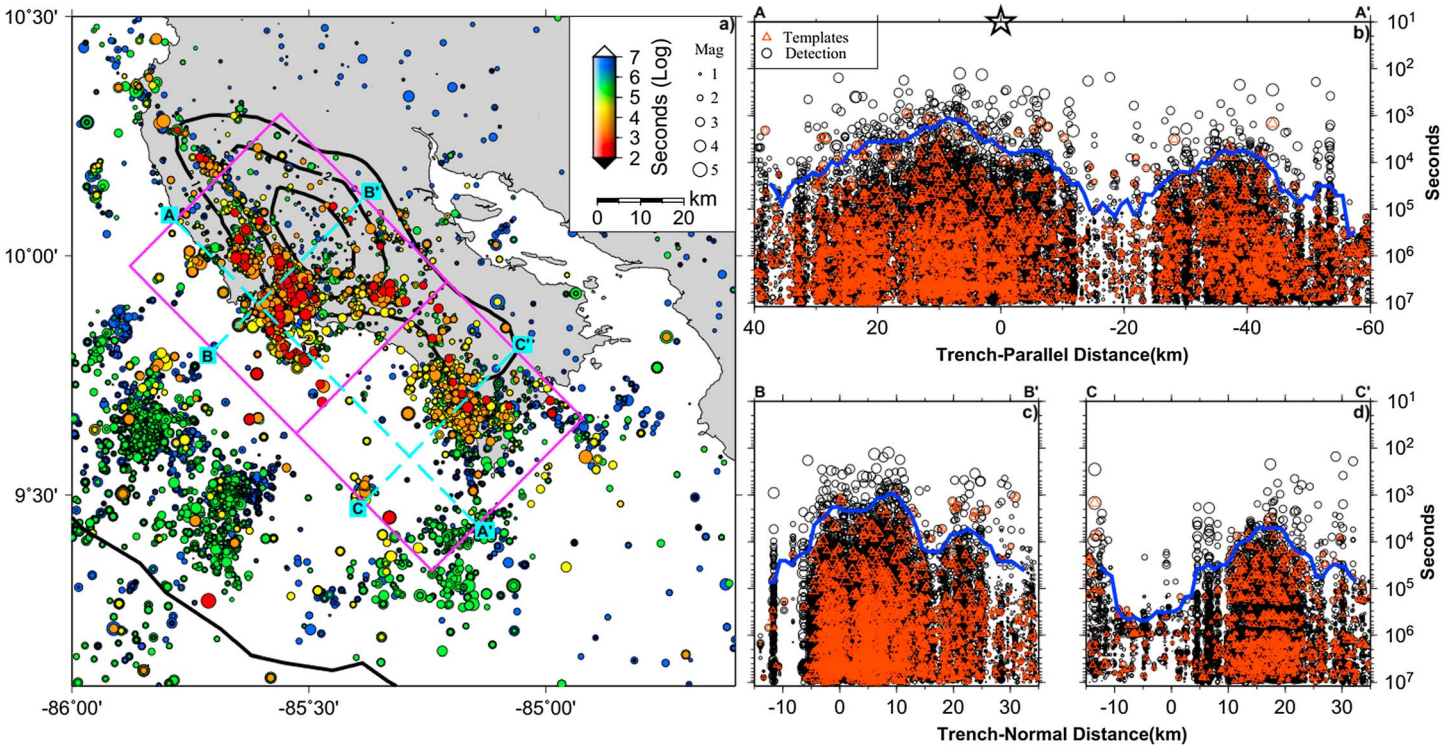


**Figure 6.** Migration of the 2012 Nicoya aftershocks. (a) Map view of all the detected events color coded by the logarithmic time after the main shock (white star). The thick black contours denotes the 1 m coseismic slip [*Kyriakopoulos and Newman*, 2016]. (b) The occurrence times of aftershocks since 2012 Nicoya main shock (open black thick star) versus trench-parallel distances (AA′). The black circles and red triangles mark the events listed in the template catalog and detected by the match filter technique, respectively. Blue thick line indicates the activation of aftershock, following *Kato and Obara* [2014]. (c) The occurrence times of aftershocks within the earthquake group to the northwest since the main shock versus trench-normal distances (BB′). (d) The same as Figure 6c for the earthquake group to the southeast (CC′).

offshore seismicity (with depths between 10 and 15 km, Figures 3d and 3e) as well as a clear cutoff edge for seismicity to the northwest (Figure 1b). While the main zones of aftershock seismicity were active seconds to minutes after the main shock, the seismicity close to the trench (depth $< 10$ km) became activated a few days after the main shock.

### 4.3. Repeating Pairs and Clusters

We initially identified repeating clusters as detection pairs with mean CC values above 0.9. Figure 7 shows an example repeating pair with the mean CC value of 0.96. For this particular pair of events, the corresponding magnitudes are $M_L$ 1.1 and $M_L$ 1.2, and their source separation after HypoDD relocation is less than 20 m. About 1170 repeating pairs were identified, which were further grouped into 53 clusters with ~370 earthquakes (Table S3), each of them containing at least four events. Figure 8 shows an example cluster of earthquakes occurring immediately offshore and near station SAJU. The waveforms recorded by the vertical component are highly similar (Figure 8a). Likewise, after relocation the source patches for events within the cluster nearly overlap (Figure 8d), based on the model assumptions described in section 3, indicating that they are indeed repeating earthquakes occurring at the same source region. Similar to previous observations [*Schaff et al.*, 1998; *Peng et al.*, 2005], their recurrence times increase systematically with time since the main shock, with an apparent Omori law decay constant, $p = 0.77$ (Figure 8c).

Figure 9a shows the locations of all repeating earthquake clusters and afterslip through the end of 2012, while the spatiotemporal distribution of regular and repeating aftershocks along the trench-parallel direction can be found in Figure 10a. We found that most repeating clusters occurred in areas that are near the edge of or areas that are largely devoid of modeled afterslip patches (Figure 9a). Most repeating clusters occurred on or near a linear dipping feature likely defining the seismogenic plate interface (Figures 9b–9f). Lastly, we found some repeating clusters became activated again following the largest $M_w$ 6.4 aftershock (Figure 10a).

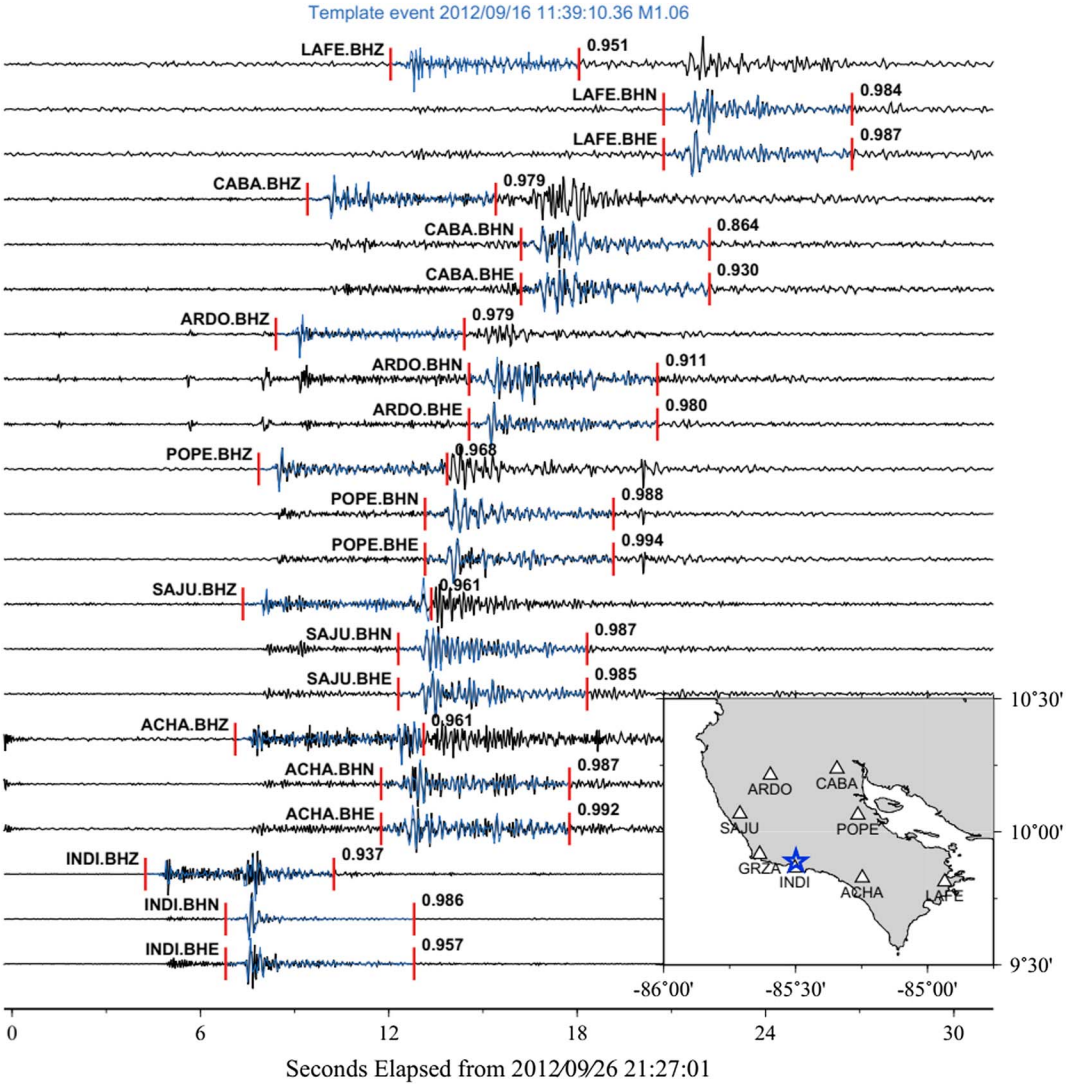


**Figure 7.** A repeating pair example. A M1.2 event 26 September 2012 21:27:02 (gray waveform) was detected by the M1.1 template 16 September 2012 11:39:12.98 (blue waveform). Station/channel and corresponding CC values are labeled. The inset map shows the template location and nearby stations.

A set of repeating earthquakes were also recorded after one of the largest aftershocks ($M_w$ 5.4) with on 23 June 2013 [*Protti et al.*, 2013].

We find a general pattern of repeating clusters occurring very near the main shock rupture patches immediately following the main shock, which consequently tend to have larger cumulative slip (maximum of ~60 mm; Figures 10b and S5 and Table S4). In contrast, clusters further from the main shock rupture exhibited some delay are less frequent and tend to have lower cumulative slip.

## 5. Discussion

High-precision aftershock relocation using a well-constrained velocity model beneath the Nicoya Peninsula [*Moore-Driskell et al.*, 2013], together with waveform matching detections, results in an unprecedented spatiotemporal profile of the aftershock evolution following the 2012 Nicoya main shock. Comparing these results to the most up-to-date images of the geodetically constrained coseismic slip and afterslip yield further insight into postseismic fault behavior.

In this study, we observed anticorrelation between dominant coseismic slip (>3 m) and aftershock density following the 2012 Nicoya main shock (Figure 1b). In particular, aftershocks mostly occurred within the updip

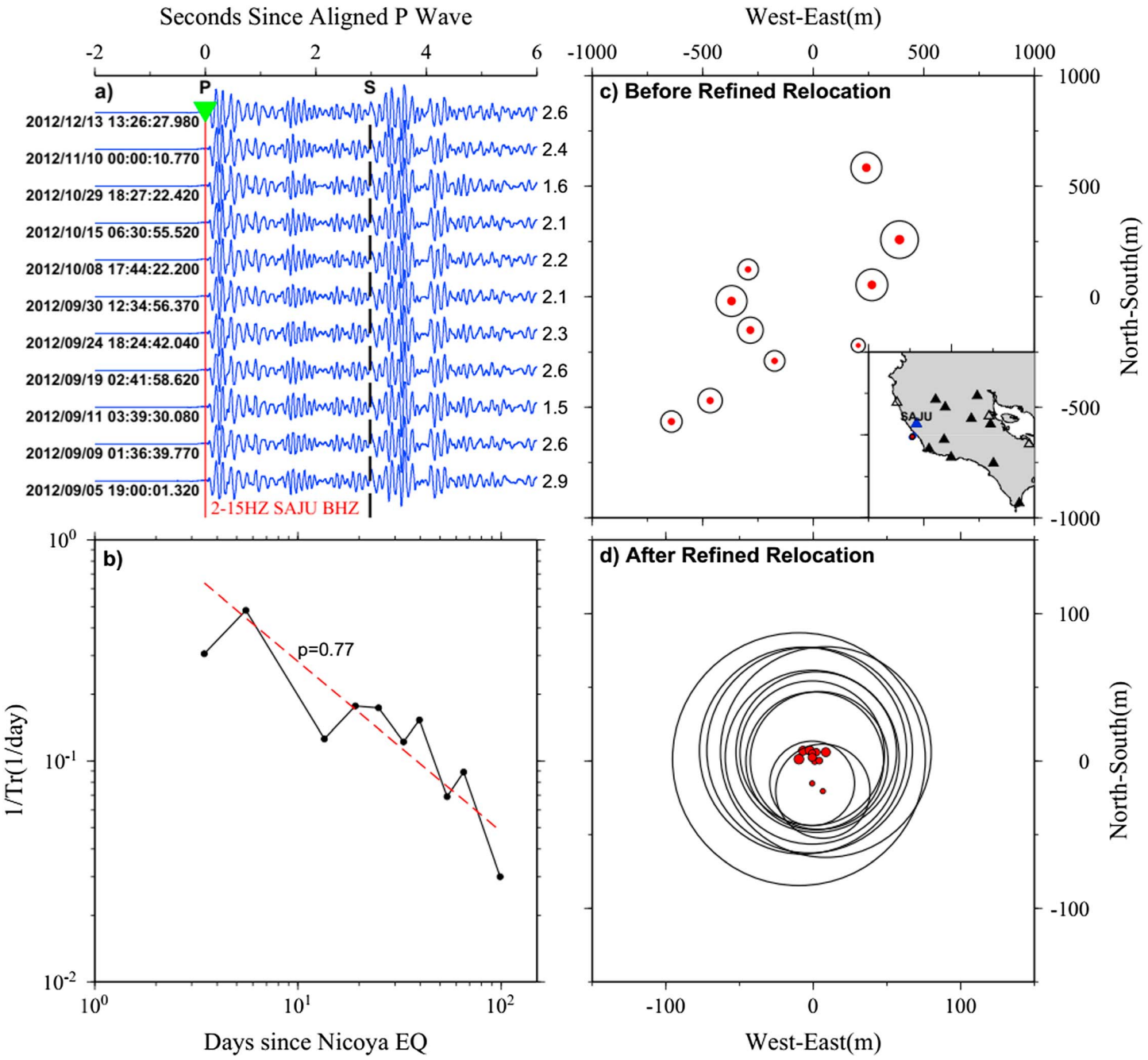


**Figure 8.** An example of a repeating cluster. (a) Vertical component waveforms recorded by station SAJU. Event origin time and magnitude are marked to the left and right, respectively. *P* and *S* phases are labeled as thin red and thicker dashed black lines. (b) With time from the main shock, the inverse of the repeating cluster recurrence interval ($T_r$) is showed to roughly follow an Omori-type power law with $p = 0.77$. (c and d) Locations of all events before and after HypoDD refined relocations.

patch of the coseismic slip area (15–20 km depth). The overall pattern of aftershocks in this study was similar to those found elsewhere [e.g., *Schaff et al*., 2002; *Thurber et al*., 2006; *Hsu et al*., 2006]. For example, following the 2005 $M_w$ 8.6 Nias-Simeulue Sumatra earthquake, most aftershocks were found to be updip of the coseismic slip zone and along the plate interface [*Hsu et al*., 2006].

The spatial distribution between aftershocks and afterslip, together with their temporal decay patterns [*Perfettini and Avouac*, 2007] and spatial migration [*Peng and Zhao*, 2009], led to the conclusion that most aftershocks around the main shock rupture are triggered by stressing from a combination of coseismic and afterslip, with the latter more dominant in the weeks to months following the main event [*Perfettini*

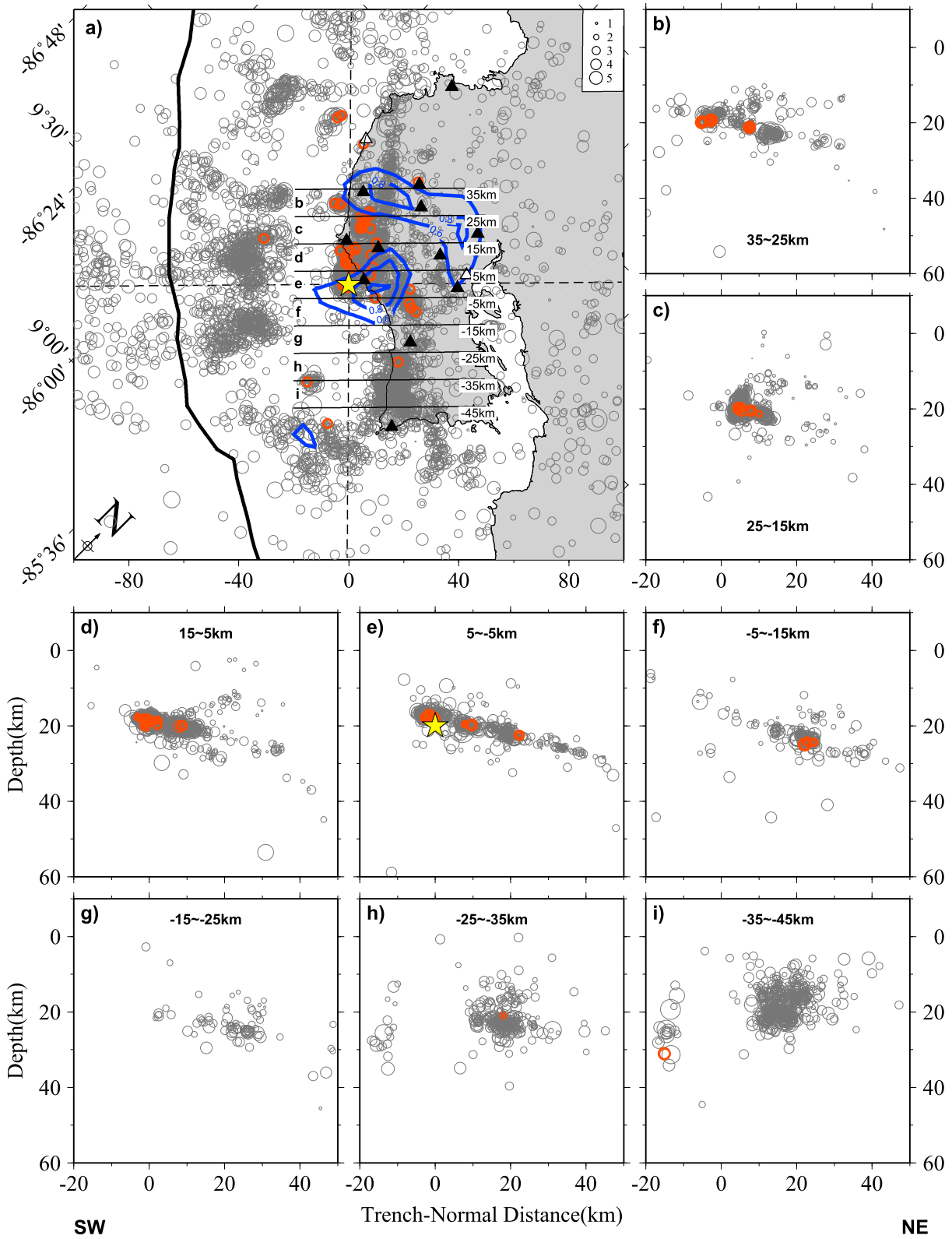


**Figure 9.** Spatial distribution of all repeating aftershock clusters. (a) Map showing the locations of all repeating clusters (red open circles), with TomoDD aftershocks plotted as gray circles. Postseismic deformation modeled as afterslip through the end of 2012 (0.25 m contours starting at 0.5 m) marked with thick blue lines [*Hobbs et al.*, 2016]. (b–i) Depth profiles and their labeling follow Figure 3.

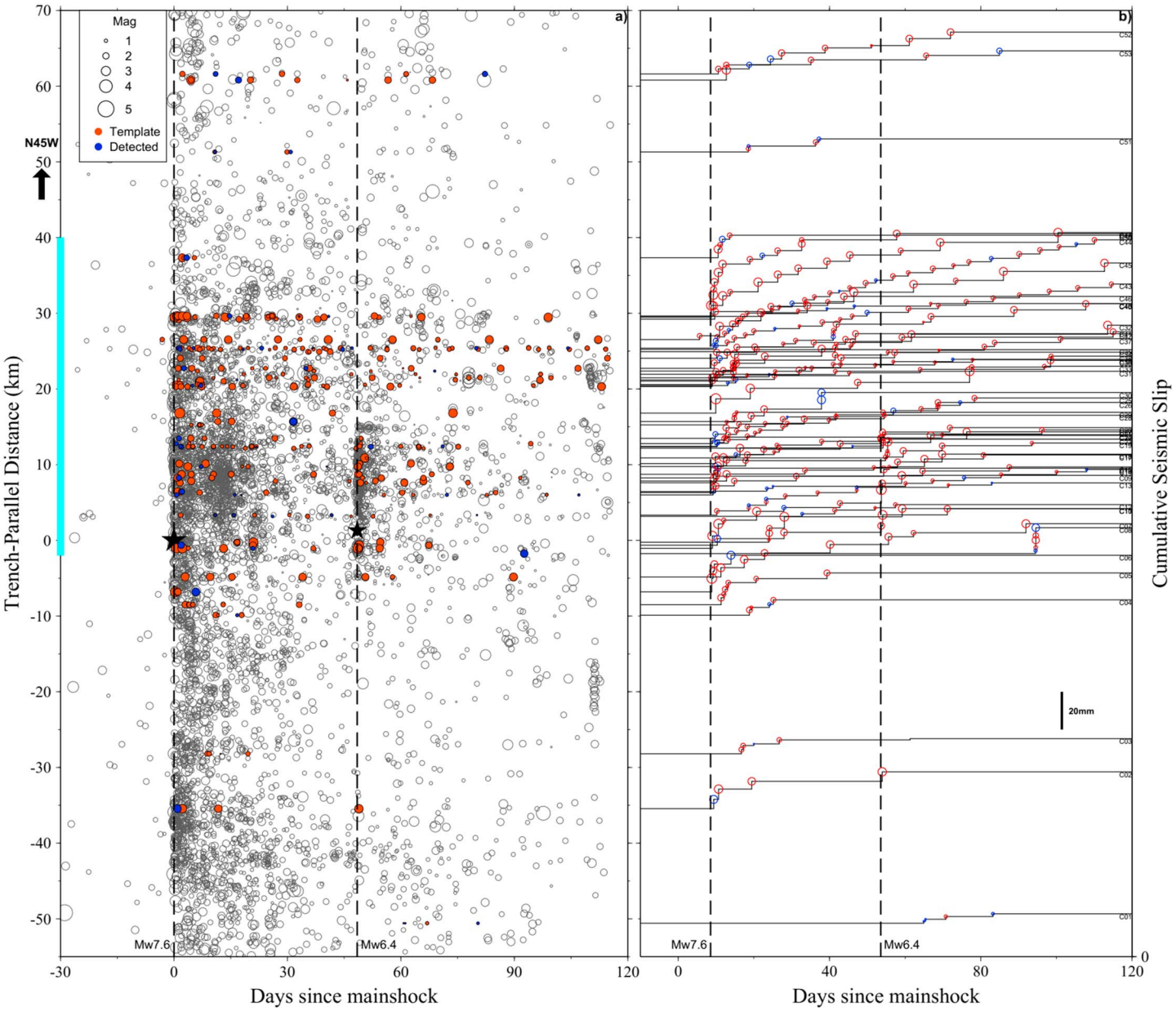


**Figure 10.** (a) Spatial-temporal distribution of relocated template catalog events (gray open circles) and repeating events for each cluster (red/blue filled circles). All events were projected along N45W centered on the main shock epicenter. Two vertical dashed lines marks the 2012 $M_w$ 7.6 Nicoya main shock and its largest $M_w$ 6.4 aftershock (black stars). Cyan bar indicates 2 m coseismic slip contours from *Kyriakopoulos and Newman* [2016]. (b) Cumulative seismic slips with times since the main shock for different clusters.

*and Avouac*, 2004]. In this study, we found that aftershocks occurred not only in regions partially overlapping the major afterslip but also among patches practically devoid of afterslip (Figure 1b). This is consistent with recent observations that both tremor and microseismicity are outside of the main slip regions during slow-slip events along the Hikurangi subduction zone in New Zealand [*Bartlow et al.*, 2014], due to static stress changes outside the slow-slip region. However, alternative models, such as pore fluid diffusion, cannot be ruled out without further detailed analysis or modeling [*Bosl and Nur*, 2002; *Hainzl et al.*, 2016].

Between the large main shock slip patches shown in Figure 1, the aftershocks tend to follow a linear dipping structure (visible in Figure 3e), which is below the interface slab model obtained before using background seismicity prior to the Nicoya main shock [*Kyriakopoulos et al.*, 2015]. While the result here is intriguing, additional relocations of both seismicity long before and after the main shock along with high-resolution seismic

tomography are needed to obtain the interface properties beneath the Peninsula, which is the subject of ongoing work [*Newman et al*., 2016]. Given minor differences found between slip models derived from the 3-D slab geometry [*Kyriakopoulos et al*., 2015], and more simple but regionally appropriate 2-D models [*Feng et al*., 2012; *Protti et al*., 2014], we do not expect that any new interface derived from these aftershock data will alter our results reported here.

Similar to other moderate to large main shocks with migrating aftershocks [*Peng and Zhao*, 2009; *Kato and Obara*, 2014; *Tang et al*., 2014], we also observed a complex expansion of aftershocks with time (Figure 6). The complexity in activation of aftershocks could be due to the fact that we simply assign the template location to the best detected event, and a better way to examine the spatiotemporal evolution may be to perform relocations for all the newly detected events. This would require additional measurements of differential travel times between tens of thousands of template and newly detected events [e.g., *Shelly et al*., 2013; *Zhang and Wen*, 2015]. Alternatively, this could be a function of the relative roughness of the plate boundary. If the Nicoya margin is controlled by medium-sized velocity-weakening asperities with along-strike heterogeneity, then it is plausible that the aftershocks simply could not expand into regions of the plate interface that are velocity-strengthening, occasionally hosting slow-slip events [e.g., *Walter et al*., 2011, 2013; *Dixon et al*., 2014].

Further supporting evidence for afterslip driving aftershocks around the epicenter is the identification of repeating aftershock clusters (Figure 9). As mentioned before, repeating earthquakes represent velocity-weakening asperities repeatedly ruptured with the recurrence interval determined by the tectonic loading rate, while the surrounding velocity-strengthening region slips aseismically [*Beeler et al*., 2001; *Matsuzawa et al*., 2004]. After the main shock, significant afterslip would change the loading patterns of those asperities and generate repeating aftershocks with rapid reduction of recurrence intervals [*Schaff et al*., 1998; *Peng et al*., 2005; *Peng and Ben-Zion*, 2006], which was identified right after the 2012 Nicoya main shock (Figure 10). Most repeating clusters were within the group around the updip edge of the major coseismic patch (Figure 9) and occurred much more frequently following the $M_w$ 7.6 main shock and the $M_w$ 6.4 largest aftershock that occurred one month later (Figure 10). We also found the most repeaters occurred along the plate interface (Figure 9), consistent with them being driven by afterslip of the same fault plane following the main shock rupture [*Igarashi et al*., 2003].

On the other hand, very few repeating clusters occurred within the second group 50 km to the southeast, where the seismicity rate recorded by CRSEIZE project [*Newman et al*., 2002; *Schwartz and DeShon*, 2007; *Ghosh et al*., 2008] was characterized as high, though during a time period long before the main shock. Although fewer stations were in operation near this group (Figure 1), at least five sites were continuously recording (PNCB, LAFE, ACHA, INDI, and POPE) within 50 km of the diffuse seismicity; thus, it is likely that these events may be diffuse and not along the slab interface. This group became activated immediately following the main shock and showed expansion both along strike and along dip, similar to the group near the main shock rupture patch (Figure 6). However, no significant afterslip was observed in this region [*Hobbs et al*., 2016], indicating alternatively mechanisms contribute to the activation and evolution of the SE cluster.

During the afterslip period, the cumulative seismic slip for repeating clusters in the along-trench parallel direction, assuming $\Delta\sigma = 3$ MPa ($\Delta\varepsilon = 10^{-4}$), is generally an order of magnitude smaller than observed from geodetic inversions using continuous GPS recordings [*Hobbs et al*., 2016]. One possibility is that we significantly underestimated the regional stress drop of aftershocks. The used value is equal to what has been found as an average along global subduction zone environments [*Allmann and Shearer*, 2009]. The image is even more complicated when considering a detailed study of earlier microseismicity from *Stankova-Pursley et al*. [2011], which reported apparent stresses (median values ranging from 0.7 to 3.2 MPa in regions below the southern and northern segments of the peninsula) rather than stress drop and is harder to directly interpret. While it is generally considered that apparent stress is less than half of the stress drop [e.g., *Savage and Wood*, 1971], its actual relationship is dictated by the seismic efficiency, a parameter that relates radiated to frictional energy released during an earthquake, and is difficult to measure [*Brodsky and Kanamori*, 2004]. Alternatively, for Nicoya, if we used the moment-slip relationship for repeating earthquakes at Parkfield [*Nadeau and Johnson*, 1998], then cumulative slip from repeating earthquakes through the end of 2012 would be in a range similar to afterslip. However, this assumption would result in abnormally high stress drops for small repeating earthquakes (up to 1000 MPa), which is not in general agreement with recent

estimates from prior microseismicity [*Stankova-Pursley et al*., 2011], or from the repeating aftershocks in Nicoya Peninsula [*Bilek et al*., 2015]. Recent studies suggest that the velocity-weakening asperities responsible for generating repeating earthquakes could also slip aseismically between adjacent events in each repeating cluster [*Beeler et al*., 2001; *Chen and Lapusta*, 2009], accounting for a large portion of cumulative slip on the asperity [*Chen and Lapusta*, 2009]. If so, this could explain the differences between cumulative seismic slip and geodetically inferred afterslip. Further analysis of trench-parallel stress drop variations for repeating clusters and the relationship with postseismic slip can better illuminate this relationship.

## 6. Conclusions

We revealed detailed patterns of aftershock behavior following the 2012 Nicoya main shock, utilizing more complete phase arrivals and an updated 3-D velocity model. The main group of aftershocks is immediately updip of the major coseismic patch, and in regions partially overlapped with afterslip. The depth distribution profile indicates that events within this group mainly occurred along the plate interface. Another group was observed 50 km to the southeast of the above cluster, where little coseismic slip or afterslip were found. Unlike the main group, earthquakes distributed across a wide range of depths within this group, possibly due to the subducted seamounts. Offshore aftershock activity, which initiated days after the main shock, was also identified.

Using the waveform matching technique, 17 times more aftershocks were found, which significantly improved the completeness of the initial catalog. The early aftershock detection results show dominantly plate interface seismicity in the first hour, while other regions were activated following that. A complex aftershock expansion pattern is reported, revealing potential trench-parallel frictional heterogeneity. Among those newly detected aftershocks, we identified 53 repeating clusters on the plate interface, which could be loaded by nearby afterslip. Most clusters initiated after the main shock, with a general pattern of rapid occurrence at early times and gradual decay with time.

**Acknowledgments**

This study was supported by the National Science Foundation grants NSF-1262267, NSF-1321552, and NSF-1447104. The seismic data of network YZ (http://www.fdsn.org/networks/detail/YZ_2009/) [*Schwartz et al*., 2009] is obtained from IRIS DMC (http://ds.iris.edu/mda/YZ?timewindow=2012-2013) and processed with the Antelope software and SAC. Figures were created using Generic Mapping Tools [*Wessel and Smith*, 1991]. This work used the Extreme Science and Engineering Discovery Environment (XSEDE) [*Towns et al*., 2014], which is supported by National Science Foundation grant ACI-1053575. Supporting data include four tables and can be obtained from the Nicoya Seismic Cycle Observatory (NSCO, http://nicoya.eas.gatech.edu) Data Product Repository.

## References

Allen, R. V. (1982), Automatic phase pickers: Their present use and future prospects, *Bull. Seismol. Soc. Am.*, *72*, S225–S242.

Allmann, B. P., and P. M. Shearer (2009), Global variations of stress drop for moderate to large earthquakes, *J. Geophys. Res.*, *114*, B01310, doi:10.1029/2008JB005821.

Bartlow, N. M., L. M. Wallace, R. J. Beavan, S. Bannister, and P. Segall (2014), Time-dependent modeling of slow slip events and associated seismicity and tremor at the Hikurangi subduction zone, New Zealand, *J. Geophys. Res. Solid Earth*, *119*, 734–753, doi:10.1002/2013JB010609.

Beeler, N. M., D. A. Lockner, and S. H. Hickman (2001), A simple stick-slip and creep slip model for repeating earthquakes and its implication for micro-earthquakes at Parkfield, *Bull. Seismol. Soc. Am.*, *91*, 1797–1804.

Ben-Zion, Y. (2003), Appendix 2. Key formulas in earthquake seismology, in *The IASPEI International Handbook of Earthquake and Engineering Seismology, Part B*, edited by W. H. K. Lee et al., pp. 1857–1875, Academic Press, London.

Ben-Zion, Y., and L. Zhu (2002), Potency-magnitude scaling relations for southern California earthquakes with $1.0 < Ml < 7.0$, *Geophys. J. Int.*, *148*, F1–F5.

Beroza, G. C., and S. Ide (2011), Slow earthquakes and nonvolcanic tremor, *Annu. Rev. Earth Planet. Sci.*, *39*, 271–296, doi:10.1146/annurev-earth-040809-152531.

Bilek, S., W. Phillips, J. Walter, Z. Peng, S. Schwartz, M. Brudzinski, and D. Yao (2015), Source parameters for repeating earthquakes along the Middle America Trench (invited), Abstract S44A-01 presented at 2015 Fall Meeting, AGU, San Francisco, Calif., 14–18 Dec.

Bosl, W. J., and A. Nur (2002), Aftershocks and pore fluid diffusion following the 1992 Landers earthquake, *J. Geophys. Res.*, *107*(B12), 2366, doi:10.1029/2001JB000155.

Brodsky, E. E., and H. Kanamori (2004), The physics of earthquakes, *Rep. Prog. Phys.*, *67*(8), 1429–1496.

Brown, J. R., G. C. Beroza, S. Ide, K. Ohta, D. R. Shelly, S. Y. Schwartz, W. Rabbel, M. Thorwart, and H. Kao (2009), Deep low-frequency earthquakes in tremor localize to the plate interface in multiple subduction zones, *Geophys. Res. Lett.*, *36*, L19306, doi:10.1029/2009GL040027.

Chen, T., and N. Lapusta (2009), Scaling of small repeating earthquakes explained by interaction of seismic and aseismic slip in a rate and state fault model, *J. Geophys. Res.*, *114*, B01311, doi:10.1029/2008JB005749.

DeMets, C., R. G. Gordon, and D. F. Argus (2010), Geologically current plate motions, *Geophys. J. Int.*, *181*, 1–80, doi:10.1111/j.1365-246X.2009.04491.x.

DeShon, H. R., S. Y. Schwartz, A. V. Newman, V. González, M. Protti, L. M. Dorman, T. H. Dixon, D. E. Sampson, and E. R. Flueh (2006), Seismogenic zone structure beneath the Nicoya Peninsula, Costa Rica, from three-dimensional local earthquake *P*- and *S*-wave tomography, *Geophys. J. Int.*, *164*(1), 109–124.

Dixon, T. H., S. Y. Schwartz, J. M. Protti, V. González, A. V. Newman, J. Marshall, and J. Spotila (2013), Detailed data available for recent Costa Rica earthquake, *EOS Trans. Am. Geophys. Union.*, *94*(2), 17–18, doi:10.1002/2013EO02.

Dixon, T. H., Y. Jiang, R. Malservisi, R. McCaffrey, N. Voss, M. Protti, and V. Gonzalez (2014), Earthquake and tsunami forecasts: Relation of slow slip events to subsequent earthquake rupture, *Proc. Nat. Acad. Sci.*, *111*(48), 17,039–17,044, doi:10.1073/pnas.1412299111.

Evans, J. R., D. Eberhart-Phillips, and C. H. Thurber (1994), User's manual for SIMULPS12 for imaging Vp and Vp/Vs: A derivative of the "Thurber" tomographic inversion SIMUL3 for local earthquakes and explosions, *U.S. Geol. Surv. Open File Rep., 94-431*

Felzer, K. R., R. E. Abercrombie, and G. Ekstrom (2003), Secondary after-shocks and their importance for aftershock forecasting, *Bull. Seismol. Soc. Am.*, *93*, 1433–1448.
Feng, L., A. V. Newman, M. Protti, V. González, Y. Jiang, and T. H. Dixon (2012), Active deformation near the Nicoya Peninsula, northwestern Costa Rica, between 1996 and 2010: Interseismic megathrust coupling, *J. Geophys. Res.*, *117*, B06407, doi:10.1029/2012JB009230.
Freed, A. (2005), Earthquake triggering by static, dynamic, and postseismic stress transfer, *Annu. Rev. Earth Planet. Sci.*, *33*, doi:10.1146/annurev.earth.33.092203.122505.
Ghosh, A., A. V. Newman, A. M. Thomas, and G. T. Farmer (2008), Interface Locking along the Subduction Megathrust from Microseismicity near Nicoya, Costa Rica, *Geophys. Res. Lett.*, *35*, L01301, doi:10.1029/2007GL031617.
Gibbons, S. J., and F. Ringdal (2006), The detection of low magnitude seismic events using array-based waveform correlation, *Geophys. J. Int.*, *165*, 149–166.
Hainzl, S. (2016), Rate-dependent incompleteness of earthquake catalogs, *Seismol. Res. Lett.*, *87*(2A), 337–344, doi:10.1785/0220150211.
Hainzl, S., T. Fischer, H. Čermáková, M. Bachura, and J. Vlček (2016), Aftershocks triggered by fluid intrusion: Evidence for the aftershock sequence occurred 2014 in West Bohemia/Vogtland, *J. Geophys. Res. Solid Earth*, *121*, 2575–2590, doi:10.1002/2015JB012582.
Harris, R. N., and K. Wang (2002), Thermal models of the Middle America Trench at the Nicoya Peninsula, Costa Rica, *Geophys. Res. Lett.*, *29*(21), 2010, doi:10.1029/2002GL015406.
Hearn, E., R. Bürgmann, and R. Reilinger (2002), Dynamics of Izmit earthquake postseismic deformation and loading of the Düzce earthquake hypocenter, *Bull. Seismol. Soc. Am.*, *92*(1), 172–193, doi:10.1785/0120000832.
Hill, D. P., and S. Prejean (2015), Dynamic triggering, in *Treatise on Geophysics*, vol. 4, 2nd ed., edited by H. Kanamori, Elsevier, Amsterdam.
Hobbs, T. E., C. Kyriakopoulos, A. V. Newman, D. Yao, T. H. Dixon, and M. Protti (2016), Recovering the Full Afterslip Following the 2012 $M_w$ 7.6 Nicoya, Costa Rica Earthquake, Abstract G51B-1097 presented at 2016 Fall Meeting, AGU, San Francisco, Calif., 12–16 Dec.
Hsu, Y., M. Simons, J.-P. Avouac, J. Galetzka, K. Sieh, M. Chlieh, D. Natawidjaja, L. Prawirodirdjo, and Y. Bock (2006), Frictional afterslip following the 2005 Nias-Simeulue earthquake, Sumatra, *Science*, *312*, 1921–1926, doi:10.1126/science.1126960.
Hutnak, M., et al. (2007), The thermal state of 18–24 Ma upper lithosphere subducting below the Nicoya Peninsula, northern Costa Rica margin, in *The Seismogenic Zone of Subduction Thrust Faults*, edited by T. Dixon and J. C. Moore, pp. 86–122, Columbia Univ. Press, New York.
Igarashi, T., T. Matsuzawa, and A. Hasegawa (2003), Repeating earthquakes and interplate aseismic slip in the northeastern Japan subduction zone, *J. Geophys. Res.*, *108*(B5), 2249, doi:10.1029/2002JB001920.
Jiang, Y., S. Wdowinski, T. H. Dixon, M. Hackl, M. Protti, and V. González (2012), Slow slip events in Costa Rica detected by continuous GPS observations, 2002–2011, *Geochem. Geophys. Geosyst.*, *13*, Q04006, doi:10.1029/2012GC004058.
Kagan, Y. Y. (2004), Short-term properties of earthquake catalogs and models of earthquake source, *Bull. Seismol. Soc. Am.*, *94*, 1207–1228.
Kanamori, H., and D. L. Anderson (1975), Theoretical basis of some empirical relations in seismology, *Bull. Seismol. Soc. Am.*, *65*, 1073–1095.
Kasahara, K. (1981), *Earthquake Mechanics*, Cambridge Univ. Press, New York.
Kato, A., and T. Igarashi (2012), Regional extent of the large coseismic slip zone of the 2011 $M_w$ 9.0 Tohoku-Oki earthquake delineated by on-fault aftershocks, *Geophys. Res. Lett.*, *39*, L15301, doi:10.1029/2012GL052220.
Kato, A., and S. Nakagawa (2014), Multiple slow-slip events during a foreshock sequence of the 2014 Iquique, Chile $M_w$ 8.1 earthquake, *Geophys. Res. Lett.*, *41*, 5420–5427, doi:10.1002/2014GL061138.
Kato, A., and K. Obara (2014), Step-like migration of early aftershocks following the 2007 $M_w$ 6.7 Noto-Hanto earthquake, Japan, *Geophys. Res. Lett.*, *41*, 3864–3869, doi:10.1002/2014GL060427.
Kato, A., K. Obara, T. Igarashi, H. Tsuruoka, S. Nakagawa, and N. Hirata (2012), Propagation of slow slip leading up to the 2011 $M_w$ 9.0 Tohoku-Oki earthquake, *Science*, *335*, 705–708, doi:10.1126/science.1215141.
King, G. C. P., and M. H. Devès (2015), Fault interaction, earthquake stress changes and the evolution of seismicity, in *Treatise on Geophysics*, Edition: Elsevier, edited by G. Schubert, chap. 7, Oxford, doi:10.1016/B978-0-444-53802-4.00077-4.
King, G. C. P., R. S. Stein, and J. Lin (1994), Static stress changes and the triggering of earthquakes, *Bull. Seismol. Soc. Am.*, *84*, 935–953.
Kirby, S. H., and A. K. Kronenberg (1987), Rheology of the lithosphere; selected topics, *Rev. Geophys.*, *25*, 1219–1244, doi:10.1029/RG025i006p01219.
Kyriakopoulos, C., and A. V. Newman (2016), Structural Asperity focusing locking and earthquake slip along the Nicoya megathrust, Costa Rica, *J. Geophys. Res. Solid Earth*, *121*, 5461–5476, doi:10.1002/2016JB012886.
Kyriakopoulos, C., A. V. Newman, A. M. Thomas, M. Moore-Driskell, and G. T. Farmer (2015), A new seismically constrained subduction interface model for Central America, *J. Geophys. Res. Solid Earth*, *120*, 5535–5548, doi:10.1002/2014JB011859.
Lay, T. (2015), The surge of great earthquakes from 2004 to 2014, *Earth Planet. Sci. Lett.*, *409*, 133–146, doi:10.1016/j.epsl.2014.10.047.
Li, L., D. Yao, X. Meng, Z. Peng, and B. Wang (2016), Increasing seismicity in Southern Tibet following the 2015 Mw 7.8 Gorkha, Nepal earthquake, *Tectonophysics*, doi:10.1016/j.tecto.2016.08.008.
Li, Z., and Z. Peng (2016), An automatic phase picker for local earthquakes with predetermined locations: Combining a signal-to-noise ratio detector with 1D velocity model inversion, *Seismol. Res. Lett.*, *87*(6), doi:10.1785/0220160027.
Lundgren, P., M. Protti, A. Donnellan, M. Heflin, E. Hernandez, and D. Jefferson (1999), Seismic cycle and plate margin deformation in Costa Rica: GPS observations from 1994 to 1997, *J. Geophys. Res.*, *104*, 28,915–28,928, doi:10.1029/1999JB900283.
Marone, C. (1998), Laboratory-derived friction laws and their application to seismic faulting, *Annu. Rev. Earth Planet. Sci.*, *26*, 643–696.
Masterlark, T., and H. F. Wang (2002), Transient stress-coupling between the 1992 Landers and 1999 Hector Mine, California, Earthquakes, *Bull. Seismol. Soc. Am.*, *92*(4), 1470–1486, doi:10.1785/0120000905.
Matsuzawa, T., N. Uchida, T. Igarashi, T. Okada, and A. Hasegawa (2004), Repeating earthquakes and quasi-static slip on the plate boundary east off northern Honshu, Japan, *Earth Planets Space*, *56*, 803–812.
Meng, X., and Z. Peng (2014), Seismicity rate changes in the Salton Sea Geothermal Field and the San Jacinto Fault Zone after the 2010 $M_w$ 7.2 El Mayor-Cucapah earthquake, *Geophys. J. Int*, *197*(3), 1750–1762.
Meng, X., Z. Peng, and J. Hardebeck (2013), Seismicity around Parkfield correlates with static shear stress changes following the 2003 $M_w$ 6.5 San Simeon earthquake, *J. Geophys. Res. Solid Earth*, *118*, 3576–3591, doi:10.1002/jgrb.50271.
Moore-Driskell, M., H. R. DeShon, W. Rabbel, M. Thorwart, Y. Dzierma, and I. G. Arroyo (2013), Integration of arrival-time datasets for consistent quality control: A case study of amphibious experiments along the Middle America Trench, *Bull. Seismol. Soc. Am.*, *103*(5), 2752–2766, doi:10.1785/0120120274.
Nadeau, R. M., and L. R. Johnson (1998), Seismological studies at Parkfield VI: Moment release rates and estimates of source parameters for small repeating earthquakes, *Bull. Seismol. Soc. Am.*, *88*, 790–814.
Nadeau, R. M., W. Foxall, and T. V. McEvilly (1995), Clustering and periodic recurrence of microearthquakes on the San Andreas fault at Parkfield, California, *Science*, *267*, 503–507.

Newman, A. V., S. Y. Schwartz, V. Gonzalez, H. R. DeShon, J. M. Protti and L. Dorman (2002), Along-strike variability in the updip limit of the seismogenic zone below Nicoya Peninsula, Costa Rica, *Geophys. Res. Lett.*, *29*(20), 1977, doi:10.1029/2002GL015409.

Newman, A. V., D. Yao, C. Kyriakopoulos, M. Moore-Driskell, T. E. Hobbs, Z. Peng, S. Y. Schwartz, M. Protti, and V. Gonzalez (2016), The possible decapitation of a megathrust indenter: Evidence from imaging of time-dependent microseismic structures before and after the 2012 $M_w$ 7.6 Nicoya, Costa Rica, Abstract T53A-01 presented at 2016 Fall Meeting, AGU, San Francisco, Calif., 12-16 Dec.

Peltzer, G., P. Rosen, F. Rogez, and K. Hudnut (1998), Poro-elastic rebound along the landers 1992 earthquake surface rupture, *J. Geophys. Res.*, *103*(B12), 30,131–30,145, doi:10.1029/98JB02302.

Peng, Z., and J. Gomberg (2010), An integrated perspective of the continuum between earthquakes and slow-slip phenomena, *Nat. Geosci.*, *3*, 599–607, doi:10.1038/ngeo940.

Peng, Z., and P. Zhao (2009), Migration of early aftershocks following the 2004 Parkfield earthquake, *Nat. Geosci.*, *2*(12), 877–881, doi:10.1038/ngeo697.

Peng, Z., and Y. Ben-Zion (2005), Spatiotemporal variations of crustal anisotropy from similar events in aftershocks of the 1999 M7.4 İzmit and M7.1 Düzce, Turkey, earthquake sequences, *Geophys. J. Int.*, *160*, 1027–1043, doi:10.1111/j.1365-246X.2005.02569.x.

Peng, Z., and Y. Ben-Zion (2006), Temporal changes of shallow seismic velocity around the Karadere-Duzce branch of the north Anatolian fault and strong ground motion, *Pure Appl. Geophys.*, *163*, 567–599, doi:10.1007/s00024-005-0034-6.

Peng, Z., J. E. Vidale, C. Marone, and A. Rubin (2005), Systematic variations in recurrence interval and moment of repeating aftershocks, *Geophys. Res. Lett.*, *32*, L15301, doi:10.1029/2005GL022626.

Peng, Z., J. E. Vidale, and H. Houston (2006), Anomalous early aftershock decay rate of the 2004 Mw6.0 Parkfield, California, earthquake, *Geophys. Res. Lett.*, *33*, L17307, doi:10.1029/2006GL026744.

Peng, Z., J. E. Vidale, M. Ishii, and A. Helmstetter (2007), Seismicity rate immediately before and after main shock rupture from high-frequency waveforms in Japan, *J. Geophys. Res.*, *112*, B03306, doi:10.1029/2006JB004386.

Perfettini, H., and J.-P. Avouac (2004), Postseismic relaxation driven by brittle creep: A possible mechanism to reconcile geodetic measurements and the decay rate of aftershocks, application to the Chi-Chi earthquake, Taiwan, *J. Geophys. Res.*, *109*, B02304, doi:10.1029/2003JB002488.

Perfettini, H., and J.-P. Avouac (2007), Modeling afterslip and aftershocks following the 1992 Landers earthquake, *J. Geophys. Res.*, *112*, B07409, doi:10.1029/2006JB004399.

Press, W., B. Flannery, S. Teukolsky, and W. Vetterling (1986), *Numerical Recipes*, Cambridge Univ. Press, Cambridge.

Protti, M., M. F. Güendel, and E. Malavassi (2001), *Evaluación del Potencial Sísmico de la Península de Nicoya*, 1st ed., pp. 144 , Ed. Fund. Univ. Nac, Heredia, Costa Rica.

Protti, M., R. Alfaro-Diaz, G. R. Brenn, S. Fasola, A. Murillo, J. S. Marshall, and T. W. Gardner (2013), Identical aftershocks from the main rupture zone 10 months after the Mw=7.6 September 5, 2012, Nicoya, Costa Rica, earthquake, Abstract G23B-0787 presented at 2013 Fall Meeting, AGU, San Francisco, Calif., 9-13 Dec.

Protti, M., V. González, A. V. Newman, T. H. Dixon, S. Y. Schwartz, J. S. Marshall, L. Feng, J. I. Walter, R. Malservisi, and S. E. Owen (2014), Nicoya earthquake rupture anticipated by geodetic measurements of the locked plate interface, *Nat. Geosci.*, *7*(2), 117–121, doi:10.1038/ngeo2038.

Savage, J. C., and M. D. Wood (1971), The relation between apparent stress and stress drop, *Bull. Seismol. Soc. Am.*, *61*, 1381–1388.

Schaff, D. P., G. C. Beroza, and B. E. Shaw (1998), Postseismic response of repeating aftershocks, *Geophys. Res. Lett.*, *25*, 4549–4552, doi:10.1029/1998GL900192.

Schaff, D. P., G. H. R. Bokelmann, G. C. Beroza, F. Waldhauser, and W. L. Ellsworth (2002), High-resolution image of Calaveras Fault seismicity, *J. Geophys. Res.*, *107*(B9), 2186, doi:10.1029/2001JB000633.

Schwartz, S. Y., and H. R. Deshon (2007), Distinct updip limits to geodetic locking and microseismicity at the northern Costa Rica seismogenic zone: Evidence for two mechanical transitions, in *The Seismogenic Zone of Subduction Thrust Faults*, edited by T. Dixon and J. C. Moore, pp. 576–599 , Columbia Univ. Press, New York.

Schwartz, S. Y., and J. M. Rokosky (2007), Slow slip events and seismic tremor at circum-Pacific subduction zones, *Rev. Geophys.*, *45*, RG3004, doi:10.1029/2006RG000208.

Schwartz, S. Y., A. V. Newman, M. Protti and V. Gonzalez (2009), Nicoya seismogenic zone. International Federation of Digital Seismograph Networks. Other/seismic network, doi:10.7914/SN/YZ_2009.

Shelly, D. R., D. P. Hill, F. Massin, J. Farrell, R. B. Smith, and T. Taira (2013), A fluid-driven earthquake swarm on the margin of the Yellowstone caldera, *J. Geophys. Res. Solid Earth*, *118*, 4872–4886, doi:10.1002/jgrb.50362.

Shelly, D., G. Beroza, and S. Ide (2007), Non-volcanic tremor and low-frequency earthquake swarms, *Nature*, *446*(7133), 305–307.

Skoumal, R. J., M. R. Brudzinski, B. S. Currie, and J. Levy (2014), Optimizing multi-station earthquake template matching through re-examination of the Youngstown, Ohio, sequence, *Earth Planet. Sci. Lett.*, *405*, 274–280, doi:10.1016/j.epsl.2014.08.033.

Stankova-Pursley, J., S. L. Bilek, W. S. Phillips, and A. V. Newman (2011), Along-strike variations of earthquake apparent stress at the Nicoya Peninsula, Costa Rica, subduction zone, *Geochem. Geophys. Geosyst.*, *12*, Q08002, doi:10.1029/2011GC003558.

Stein, R. S., G. C. P. King, and J. Lin (1994), Stress triggering of the 1994 M = 6.7 Northridge, California, earthquake by its predecessors, *Science*, *265*, 1432–1435.

Stein, R. S., A. A. Barka, and J. H. Dieterich (1997), Progressive failure on the North Anatolian fault since 1939 by earthquake stress triggering, *Geophys. J. Int.*, *128*, 594–604.

Tang, C.-C., C.-H. Lin, and Z. Peng (2014), Spatio-temporal evolutions of early aftershocks following te 2010 ML 6.4 Jiashian earthquake in Southern Taiwan, *Geophys. J. Int.*, *199*, 1772–1783, doi:10.1093/gji/ggu361.

Thurber, C., H. Zhang, F. Waldhauser, J. Hardebeck, A. Michael, and D. Eberhart-Phillips (2006), Three-dimensional compressional wavespeed model, earthquake relocations, and focal mechanisms for the Parkfield, California, region, *Bull. Seismol. Soc. Am.*, *96*, 38–49.

Toda, S., R. Stein, G. Beroza, and D. Marsan (2012), Aftershocks halted by static stress shadows, *Nat. Geosci.*, *5*(6), 410–413.

Towns, J., et al. (2014), XSEDE: Accelerating scientific discovery, *Comput. Sci. Eng.*, *16*(5), 62–74, doi:10.1109/MCSE.2014.80.

Waldhauser, F., and W. L. Ellsworth (2000), A double-difference earthquake location algorithm: Method and application to the northern Hayward Fault, California, *Bull. Seismol. Soc. Am.*, *90*, 1353–1368, doi:10.1785/0120000006.

Walter, J. I., S. Y. Schwartz, J. M. Protti, and V. Gonzalez (2011), Persistent tremor within the northern Costa Rica seismogenic zone, *Geophys. Res. Lett.*, *38*, L01307, doi:10.1029/2010GL045586.

Walter, J. I., S. Y. Schwartz, M. Protti, and V. Gonzalez (2013), The synchronous occurrence of shallow tremor and very low frequency earthquakes offshore of the Nicoya Peninsula, Costa Rica, *Geophys. Res. Lett.*, *40*, 1517–1522, doi:10.1002/grl.50213.

Walter, J. I., X. Meng, Z. Peng, S. Y. Schwartz, A. V. Newman, and M. Protti (2015), Far-field triggering of foreshocks near the nucleation zone of the 5 September 2012 ($M_W$ 7.6) Nicoya Peninsula, Costa Rica earthquake, *Earth Planet. Sci. Lett.*, *431*, 75–86, doi:10.1016/j.epsl.2015.09.017.

Wessel, P., and W. Smith (1991), Free software helps map and display data, *Eos Trans. AGU*, *72*(441), 445–446.
Wu, C., X. Meng, Z. Peng, and Y. Ben-Zion (2014), Lack of spatiotemporal localization of foreshocks before the 1999 $M_w$ 7.1 Düzce, Turkey, earthquake, *Bull. Seismol. Soc. Am.*, *104*(1), 560–566.
Yao, D., Z. Peng, and X. Meng (2015), Systematical search for remotely triggered earthquakes in Tibetan Plateau following the 2004 *M* 9.0 Sumatra and 2005 *M* 8.6 Nias earthquakes, *Geophys. J. Int.*, *201*(2), 543–551, doi:10.1093/gji/ggv037.
Yue, H., T. Lay, S. Y. Schwartz, L. Rivera, M. Protti, T. H. Dixon, S. Owen, and A. V. Newman (2013), The 5 September 2012 Nicoya, Costa Rica $M_w$ 7.6 earthquake rupture process from joint inversion of high-rate GPS, strong-motion, and teleseismic P wave data and its relationship to adjacent plate boundary interface properties, *J. Geophys. Res. Solid Earth*, *118*, 5453–5466, doi:10.1002/jgrb.50379.
Zhang, H., and C. H. Thurber (2003), Double-difference tomography: The method and its application to the Hayward fault, California, *Bull. Seismol. Soc. Am.*, *93*, 1875–1889.
Zhang, M., and L. Wen (2015), An effective method for small event detection: Match and locate (M&L), *Geophys. J. Int.*, *200*(3), 1523–1537.